Cysteine-Mediated Aggregation of Au Nanoparticles: The Development of a H_2O_2 Sensor and Oxidase-Based Biosensors

Fuan Wang, Xiaoqing Liu, Chun-Hua Lu, and Itamar Willner*

Institute of Chemistry, The Center for Nanoscience and Nanotechnology, The Hebrew University of Jerusalem, Jerusalem 91904, Israel

ABSTRACT The cysteine-stimulated aggregation of Au nanoparticles (Au NPs) is used as an auxiliary reporting system for the optical detection of H_2O_2, for optical probing of the glucose oxidase (GOx) and the catalyzed oxidation of glucose, for probing the biocatalytic cascade composed of acetylcholine esterase/choline oxidase (AChE/ChOx), and for following the inhibition of AChE. The analytical paradigm is based on the I^--catalyzed oxidation of cysteine by H_2O_2 to cystine, a process that prohibits the cysteine-triggered aggregation of the Au NPs. The system enabled the analysis of H_2O_2 with a detection limit of 2 μM. As the GOx-biocatalyzed oxidation of glucose yields H_2O_2, and the AChE/ChOx cascade leads to the formation of H_2O_2, the two biocatalytic processes could be probed by the cysteine-stimulated aggregation of the Au NPs. Since AChE is inhibited by 1,5-bis(4-allyldimethylammonium phenyl)pentane-3-one dibromide, the biocatalytic AChE/ChOx cascade is inhibited by the inhibitor, thus leading to the enhanced cysteine-mediated aggregation of the NPs. The results suggest the potential implementation of the cysteine-mediated aggregation of Au NPs in the presence of AChE/ChOx as a sensing platform for the optical detection of chemical warfare agents.

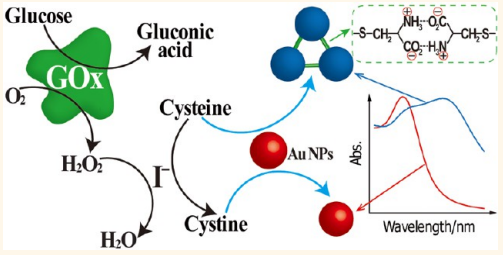

KEYWORDS: nanoparticle · aggregation · enzyme · hydrogen peroxide · oxidase · glucose · acetylcholine esterase

The aggregation of Au nanoparticles (Au NPs) and the accompanying color changes have been a subject of extensive research in the past decade, and numerous molecular or biomolecular optical sensing platforms were developed based on the aggregation principle.[1−3] The color changes observed upon aggregation of the plasmonic NPs originate from the coupling between the localized surface plasmons of the NPs that results in lower energy excitation levels and red-shifted absorbance bands.[4,5] Different motives were reported to stimulate the aggregation of Au NPs, and these included the bridging of the NPs by complementary biorecognition complexes[6−8] or host−guest interactions,[9,10] the use of complementary H-bonds[11] or donor−acceptor interactions.[12,13] Also, the decrease of the surface charge associated with NPs led to the aggregation of NPs.[14] The most extensively studied aggregated Au NP systems have involved nucleic-acid-bridged aggregation of Au NPs and the development of DNA sensing systems,[15] formation of aptamer complex systems,[16,17] T-Hg^{2+}-T duplex nucleic acids for the detection of Hg^{2+} ions,[18,19] DNAzyme-bridged Au NPs for the analysis of Pb^{2+} ions,[20] and more.[21] Also, ligand-modified Au NPs were aggregated in the presence of metal ions through the formation of interparticle metal ion complexes.[22]

Besides the aggregation phenomena of Au NPs, other sensing platforms have implemented metallic or semiconductor NPs.[23−25] For example, molecularly imprinted Au NP matrices associated with Au surfaces were used for the selective electrochemical or surface plasmon resonance (SPR) detection of different substrates.[26−28] Pt NPs were applied as electrocatalytic labels for amplified sensing, through the electrocatalyzed reduction of H_2O_2.[29] Receptor-cross-linked Au NP layers associated with electrodes were used for the selective electrochemical detection of receptor-bound analytes,[30] and functionalized semiconductor quantum dots (QDs) were applied for the

* Address correspondence to willnea@vms.huji.ac.il.

Received for review June 4, 2013 and accepted July 5, 2013.

Published online July 05, 2013
10.1021/nn402810x

optical detection of different substrates through host–guest interactions,[31] electrostatic interactions,[32,33] or donor–acceptor interactions.[34] The use of NPs for the analysis of glucose attracted specific research efforts. The discovery that H_2O_2 acts as reducing agent for the reduction of $AuCl_4^-$ to Au^0 and the enlargement of Au NPs seeds was used to develop an optical glucose sensing platform by the glucose oxidase (GOx)-catalyzed oxidation of glucose and the use of the generated H_2O_2 for growing Au NPs.[35−37] Similarly, semiconductor QDs were applied for the optical detection of H_2O_2 that oxidizes the QDs' surface to traps that quench the luminescence of the QDs. This process was applied for glucose sensing by the GOx-catalyzed oxidation of glucose to gluconic acid and H_2O_2 and the utilization of the latter product as reactant that leads to the quenching of the luminescence of the QDs.[38−40] Direct optical sensing of glucose was demonstrated by imprinted phenylboronic-acid-functionalized Au NPs associated with Au surface using SPR as the readout signal for the association of glucose to the imprinted sites.[41]

In the present study, we implement the cysteine-mediated aggregation of Au NPs as the basic process for the sensitive detection of H_2O_2. We then use the H_2O_2 sensing platform for the analysis of glucose in the presence of GOx and for the detection of chemical warfare by detecting an inhibitor of acetylcholine esterase (AChE) using the acetylcholine esterase/choline oxidase (AChE/ChOx) biocatalytic cascade.

RESULTS AND DISCUSSION

Cysteine stimulates the aggregation of Au NPs through the formation of interparticle H-bonds and zwitterionic electrostatic interactions[42,43] (Figure 1A). Accordingly, rapid aggregation proceeds, leading to a color change from the red color of the individual Au NPs to the violet color corresponding to the aggregated NPs. The aggregation was also reflected in the ultraviolet/visible (UV/vis) spectrum of the Au NPs, with the decrease in absorption at 520 nm and the production of a new absorption peak at 650 nm. Figure 1B shows the time-dependent absorbance changes upon interaction of the Au NPs (100 μL; 12 nM) with cysteine (100 μL; 20 μM) (for details, see Figure S1, Supporting Information). Figure 1C depicts the spectral changes upon subjecting the Au NPs to different concentrations of cysteine for a fixed time interval of 10 min and the absorbance changes associated with the derived calibration curve (Figure 1C, inset). Evidently, the aggregation of the Au NPs reaches a constant saturation value at a cysteine concentration of 10 μM for a fixed time interval corresponding to 10 min, and hence, all other experiments were conducted under this condition.

The oxidation of cysteine (**1**) to cystine (**2**) by H_2O_2 is a slow process. This reaction is catalyzed, however, by the addition of iodide ion, I^- (Figure 2A inset).

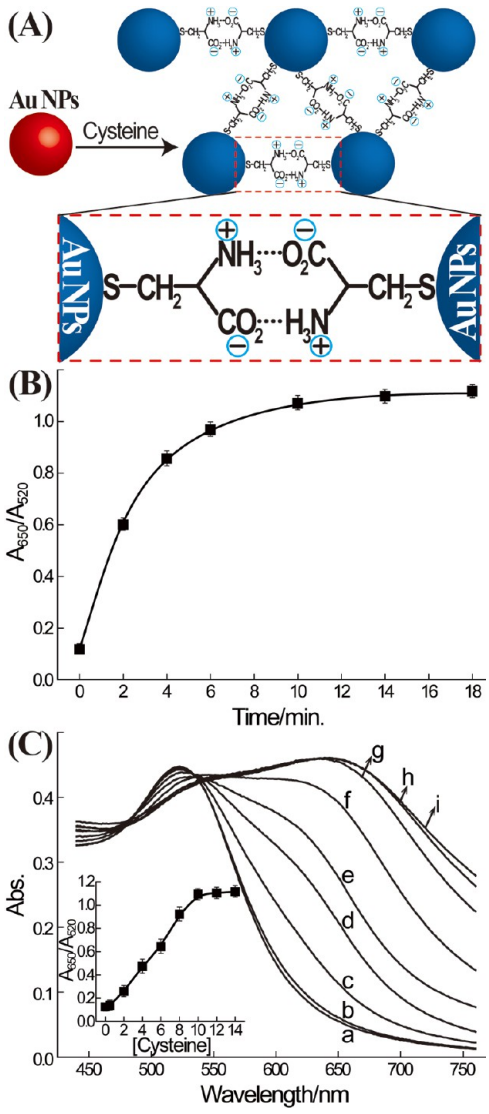

Figure 1. (A) Schematic cysteine-mediated aggregation of Au NPs. (B) Time-dependent absorbance changes of the Au NPs upon adding cysteine (100 μL; 20 μM) to the Au NPs (100 μL; 12 nM) solution. (C) Absorption spectra corresponding to the aggregation of the Au NPs in the presence of different concentrations of cysteine: (a) 0, (b) 1, (c) 2, (d) 4, (e) 6, (f) 8, (g) 10, (h) 12, and (i) 14 μM. Inset: Derived calibration curve. Spectra were recorded after a fixed time interval of 10 min. Error bars derived from a set of four experiments.

The catalytic mechanism for the I^--catalyzed oxidation of cysteine to cystine by H_2O_2 was previously reported,[44] and it is summarized and discussed in Figure S2A (Supporting Information). The I^--catalyzed oxidation of cysteine by H_2O_2 yields cystine. The resulting disulfide does not stimulate any aggregation of the Au NPs within the time scales applied for studying the different systems. The optimization of the Au-NP-mediated probing of the cysteine/I^-/H_2O_2 system is discussed in Figure S2B (Supporting Information). Control experiments show that I^- has no effect on the aggregation process of Au NPs, implying that the inhibited aggregation of Au NPs originates from the H_2O_2-mediated oxidation of cysteine to cystine (Figure S3, Supporting Information). Thus, as

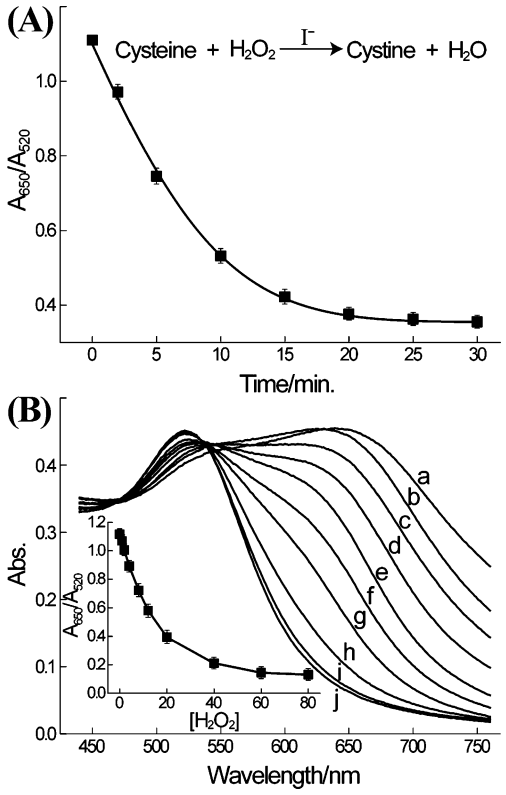

Figure 2. (A) Absorbance features corresponding to the cysteine-stimulated aggregation of the Au NPs that probe the time-dependent I^--catalyzed oxidation of cysteine (1) to cystine (2) by H_2O_2, 20 μM, and the effect of the oxidation of cysteine on the aggregation process. (B) Absorption spectra corresponding to the aggregation of the Au NPs by cysteine solutions, 20 μM, treated with different concentrations of H_2O_2 in the presence of I^-, 0.2 μM, for a fixed time interval of 20 min: (a) 0, (b) 2, (c) 4, (d) 8, (e) 12, (f) 16, (g) 20, (h) 40, (i) 60, and (j) 80 μM. Absorption spectra of the aggregated Au NPs were recorded after a fixed time interval of 10 min. Inset: derived calibration curve. Error bars derived from a set of four experiments.

the concentration of H_2O_2 decreases, the extent of oxidation of cysteine is reduced and, hence, the aggregation of the Au NPs is enhanced.

Figure 2A shows the effect of the reaction time between cysteine/I^- and H_2O_2 on the aggregation of the Au NPs (for details, see Figure S4, Supporting Information). In these experiments, the cysteine/I^- system is allowed to react with 20 μM H_2O_2 for different time intervals (leading to cystine; see Figure 2A inset), and subsequently, the Au NPs are added to the reaction mixture and the extent of the stimulated aggregation of the Au NPs is followed after a fixed time interval of 10 min. Figure 2B shows the effect of H_2O_2 concentrations on the cysteine/I^--stimulated aggregation of the Au NPs. In these experiments, the cysteine/I^- system was allowed to react with variable concentrations of H_2O_2 for a fixed time interval of 20 min, and subsequently, the Au NPs were added to the reaction mixture, and their degree of aggregation was followed spectroscopically after a fixed time interval of 10 min. The derived calibration curve between the absorbance of the aggregated Au NPs and the concentration of H_2O_2 is shown in the inset of Figure 2B. Evidently, as the concentration of H_2O_2 increases, the degree of aggregation is inhibited, as reflected in the UV/vis spectra, with a decreased absorption at 520 nm (A_{520}) and an increased absorption at 650 nm (A_{650}). The ratio of A_{650}/A_{520} decreased as the concentration of H_2O_2 increased in the cysteine/I^- reaction mixture. The system enabled the sensitive analysis of H_2O_2 with a detection limit of 2 μM.

Further support for the effect of the I^--catalyzed oxidation of cysteine to cystine by H_2O_2 on the aggregation of the Au NPs was obtained by TEM imaging of the degree of aggregation of the NPs (Figure 3). Figure 3A shows the TEM image of the original Au NPs. In Figure 3B, the TEM image of the aggregates formed by the Au NPs, in the absence of H_2O_2, yet in the presence of cysteine/I^-, is presented. Effective aggregation of Au NPs is observed, consistent with the efficient cysteine-cross-linked aggregation of the NPs. Figure 3C depicts the TEM image of the resulting Au NP aggregates formed upon the primary treatment of the cysteine solution with H_2O_2, 16 μM, in the presence of I^-, 0.2 μM, for 20 min and the subsequent treatment of the mixture with the Au NPs and allowing aggregation for a time interval of 10 min. The image shows substantially less efficient aggregation, consistent with the partial oxidation of cysteine to cystine, thus leading to only partial aggregation. Figure 3D shows the TEM image resulting upon treatment of cysteine solution in the presence of 40 μM of H_2O_2 and 0.2 μM of I^- for a time interval of 20 min, subjecting the resulting mixture to the Au NPs, and allowing their aggregation for a fixed time interval of 10 min. The TEM image reveals that most of the Au NPs exist as single NPs with some NPs revealing a very low degree of aggregation. This result is consistent with the fact that cysteine is effectively oxidized to cystine by the high concentration of H_2O_2 (in the presence of I^-), thus prohibiting the cysteine-stimulated aggregation of the NPs. It should be noted that disulfides are known to bind to Au NPs,[42] and hence, the disulfide product might also induce the aggregation of the NPs. Nonetheless, the cystine-induced aggregation of the Au NPs is substantially slower than the cysteine-mediated aggregation of the Au NPs, and it does not proceed on the time scale of the cysteine-induced aggregation process.

The successful sensitive detection of H_2O_2 was, then, implemented for the analysis of glucose. Glucose oxidase, GOx, catalyzes the oxidation of glucose by O_2 to yield gluconic acid and H_2O_2 (eq 1). The latter product, in the presence of the catalyst, I^-, oxidizes cysteine (**1**) to cystine (**2**), Figure 4A. As the concentration of H_2O_2 is controlled by the concentration of glucose, the inhibition of the cysteine-mediated aggregation of the Au NPs, in the presence of I^-,

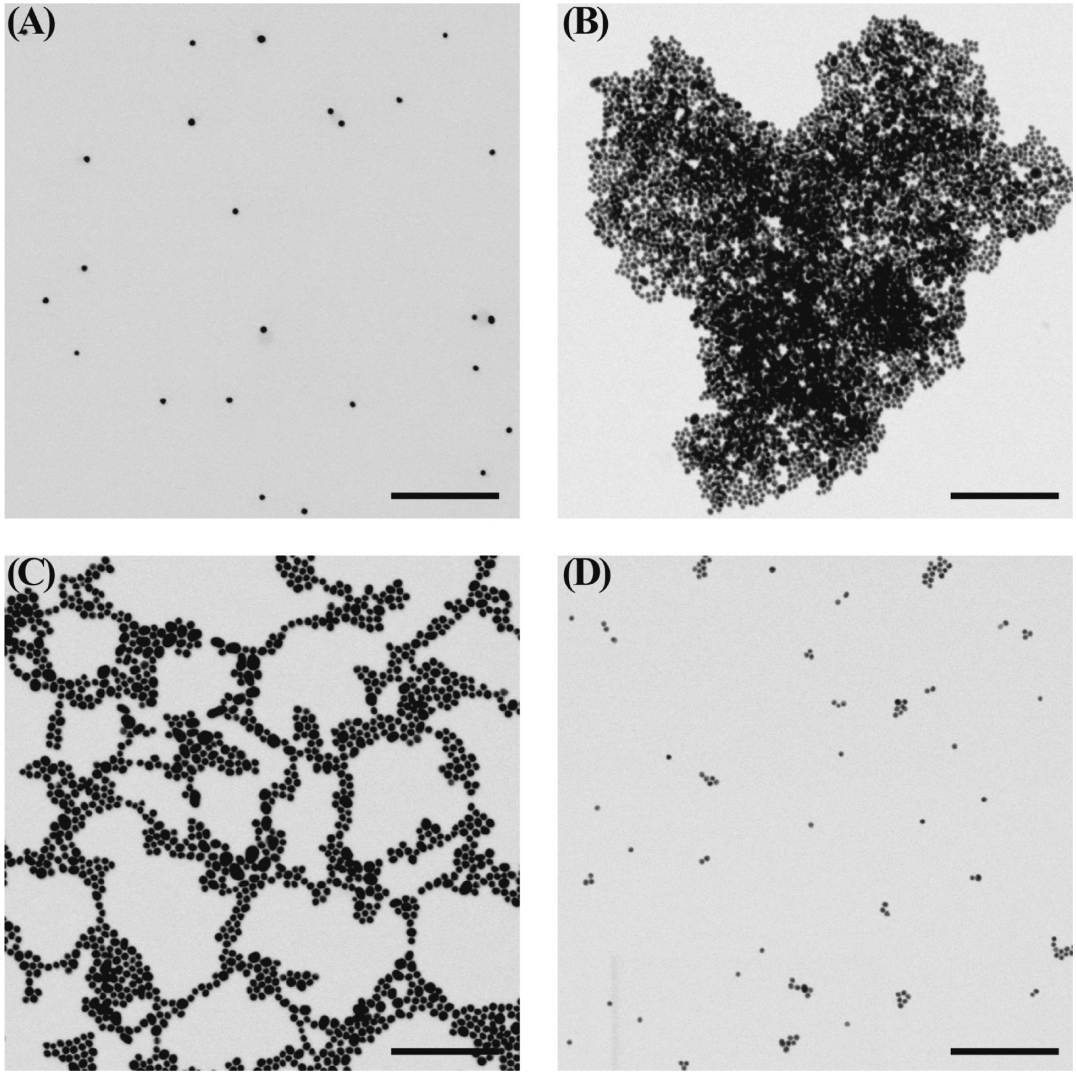

Figure 3. TEM images corresponding to the Au NP aggregates generated by cysteine treated with variable concentrations of H_2O_2: (A) Au NPs only, (B) 0 μM, (C) 16 μM, and (D) 40 μM for a time interval of 20 min (I^- concentration 0.2 μM), followed by subjecting the resulting mixtures to Au NPs, and allowing their aggregation for 10 min. Scale bars represent 250 nm.

should be dictated by the biocatalyzed oxidation of glucose.

$$\text{glucose} + O_2 \xrightarrow{\text{GOx}} \text{gluconic acid} + H_2O_2 \qquad (1)$$

Accordingly, the biocatalyzed oxidation of different concentrations of glucose by GOx was conducted for a fixed time interval, and afterward, the cysteine/I^- and Au NP reporter system was added to the GOx/glucose reaction mixture that follows the GOx-generated H_2O_2 through the Au NP aggregation process. Figure 4B exemplifies the analysis of the time-dependent formation of H_2O_2 by GOx/glucose/O_2 at a fixed concentration of glucose, 200 μM, through the secondary aggregation of the Au NPs in the presence of the cysteine/I^-/Au NP reporter system (for details, see Figure S5, Supporting Information). Figure 4C depicts the absorption spectra of the Au NPs upon analyzing different concentrations of glucose for a fixed time interval of 60 min. Evidently, as the concentration of glucose increases, the aggregation of the cysteine/I^-/Au NP reporter system is inhibited, consistent with the higher content generation of H_2O_2 that mediated the oxidation of cysteine to cystine. By monitoring the ratio of absorbance A_{650}/A_{520}, an appropriate calibration curve relating the absorbance of the aggregated Au NPs with the concentration of glucose was derived (Figure 4C inset). Control experiments revealed that in the absence of GOx or glucose, the aggregation of the NPs in the presence of cysteine/I^-/Au NP reporter system proceeded at a similar efficiency as the system without GOx and glucose, implying that GOx or glucose only do not affect the aggregation of the NPs (Figure S6, Supporting Information). These results also indicate that the inhibition of aggregated Au NPs

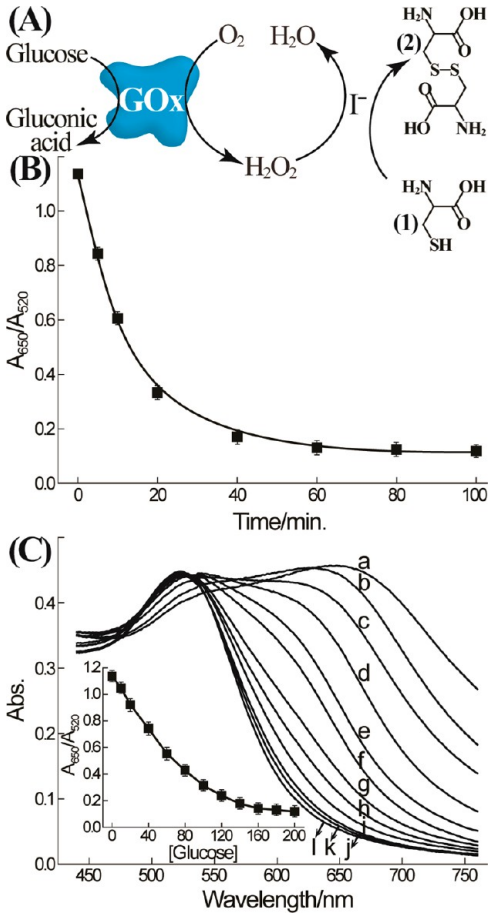

Figure 4. (A) GOx-mediated oxidation of glucose by O_2 to yield gluconic acid and H_2O_2 and the subsequent I^--catalyzed oxidation of cysteine to cystine by H_2O_2. (B) Absorbance features corresponding to the probing of the GOx-biocatalyzed oxidation of glucose through the aggregation of the Au NPs. To record the absorbance features, the GOx-catalyzed oxidation of glucose, 200 μM, is activated for different time intervals. The resulting H_2O_2-containing mixtures are subjected to the cysteine/I^- reporter system for a fixed time interval of 20 min. Subsequently, the Au NPs are added to the resulting mixtures for a fixed time interval of 10 min. (C) Absorbance spectra corresponding to the analysis of different concentrations of glucose through the aggregation of the NPs by the cysteine/I^-/Au NP reporter system. In the first step, the GOx-mediated oxidation of different concentrations of glucose is activated for a fixed time interval of 60 min: (a) 0, (b) 10, (c) 20, (d) 40, (e) 60, (f) 80, (g) 100, (h) 120, (i) 140, (j) 160, (k) 180, and (l) 200 μM. The resulting reaction mixtures were subjected to the cysteine/I^- reporter system for 20 min, and subsequently, Au NPs were added to the reaction mixtures. Spectra were recorded after allowing the aggregation of Au NPs for a fixed time interval of 10 min. Inset: resulting calibration curve. Error bars derived from a set of four experiments.

originates from the GOx/glucose/O_2-generated H_2O_2 and that this photophysical process enabled the quantitative assay of glucose.

The successful analysis of GOx/glucose by the cysteine/I^-/Au NP reporter system suggests that the present system may be implemented to follow the activation of biocatalytic cascades that involve H_2O_2-generating oxidase. This is demonstrated by following the acetylcholine esterase/choline oxidase (AChE/ChOx) bienzyme cascade and the detection of an acetylcholine esterase inhibitor as a model system for sensing chemical warfare agents. Acetylcholine is a central neurotransmitter and is involved in neurological disorders, such as schizophrenia, Tourette's syndrome, Huntington's, Parkinson's, and Alzheimer's diseases.[45] AChE-mediated hydrolysis of acetylcholine is the main regulating process of the neural response system.[46] The inhibition of AChE, for example, by nerve gases, leads to the perturbations of the nerval conduction process and to the rapid paralysis of vital functions of the living system.[47] Different colorimetric[48,49] or electrochemical methods[50] to sense the activity of AChE and following its inhibition were developed. For example, CdS semiconductor nanoparticles were coupled with AChE to yield a hybrid system that enabled the photoelectrochemical detection of AChE activity and to follow the inhibition of the enzyme.[51] Also, the colorimetric detection of AChE and its inhibition were probed by the biocatalyzed hydrolysis of thioacetylcholine and the subsequent aggregation of Au NPs by the resulting thiocholine.[52,53] Alternatively, optical detection of AChE activity was demonstrated using semiconductor CdSe/ZnS QDs. In this system, the biocatalytic cascade consisted of AChE/ChOx-generated H_2O_2, and this led to the quenching of the luminescence of the QDs.[54,55] Figure 5A depicts the method to follow the AChE/ChOx cascade. AChE catalyzes the hydrolysis of acetylcholine (**3**) into choline (**4**). The resulting choline is oxidized by O_2, in the presence of ChOx as biocatalyst, to yield betaine aldehyde (**5**), while producing H_2O_2 that is followed by the cysteine/I^-/Au NP reporter system. Figure 5B shows the analysis of the time-dependent formation of H_2O_2 by the AChE/ChOx cascade at a fixed concentration of acetylcholine, 400 μM, through the aggregation of the NPs by using the cysteine/I^-/Au NP reporter system (for details, see Figure S7, Supporting Information). Figure 5C depicts the effect of different concentrations of acetylcholine on the AChE-stimulated aggregation of the Au NPs. In these experiments, the AChE/ChOx cascade, in the presence of variable concentrations of acetylcholine, is activated for a fixed time interval of 120 min. The resulting reaction mixtures were subjected to the cysteine/I^- reporter system for 20 min, and subsequently, Au NPs were added to the reaction mixtures, and their degree of aggregation was followed spectroscopically after a fixed time interval of 10 min. Evidently, as the concentration of acetylcholine increases, the aggregation process is inhibited, consistent with the elevated amounts of H_2O_2 generated by the AChE/ChOx bienzyme cascade system. Control experiments revealed that in the presence of acetylcholine and only one of the enzymes AChE or ChOx the aggregation of the Au NPs in the presence of cysteine/I^- proceeded with an

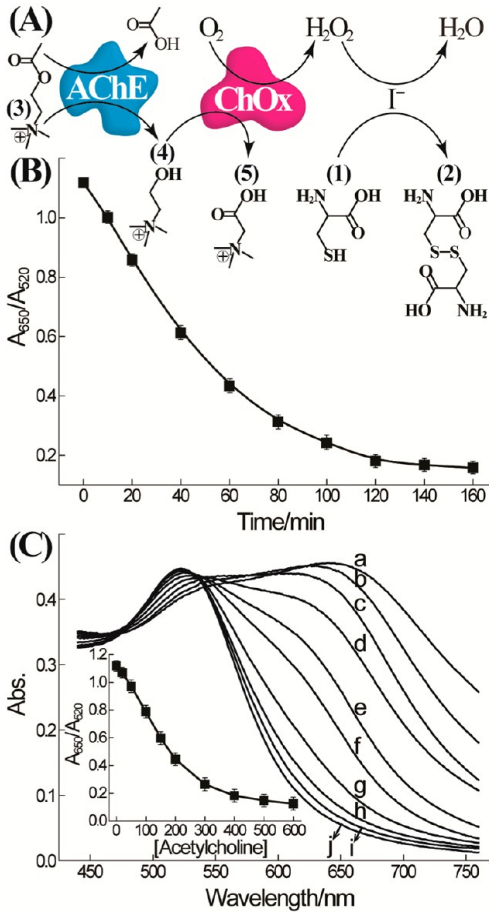

Figure 5. (A) Activation of the AChE/ChOx cascade that hydrolyzes acetylcholine (3) and oxidizes choline (4) to betaine aldehyde (5) and H_2O_2, and the subsequent I^--catalyzed oxidation of cysteine to cystine by the resulting H_2O_2. (B) Absorbance features corresponding to the probing of the cascaded AChE-mediated hydrolysis of acetylcholine to choline and ChOx-biocatalyzed oxidation of choline through the aggregation of the Au NPs. To record the absorbance features, the AChE/ChOx cascaded system is activated in the presence of acetylcholine, 400 μM, for different time intervals. The resulting H_2O_2-containing mixtures are subjected to the cysteine/I^- reporter system for a fixed time interval of 20 min. Subsequently, the Au NPs are added to the resulting mixtures, and the spectra corresponding to the aggregated Au NPs were recorded after a fixed time interval of 10 min. (C) Absorbance spectra corresponding to the analysis of different concentrations of acetylcholine through the aggregation of the NPs by the cysteine/I^-/Au NP reporter system. In the first step, the AChE/ChOx cascaded system is activated in the presence of different concentrations of acetylcholine for a fixed time interval of 120 min: (a) 0, (b) 20, (c) 50, (d) 100, (e) 150, (f) 200, (g) 300, (h) 400, (i) 500, and (j) 600 μM. The resulting reaction mixtures were subjected to the cysteine/I^- reporter system for 20 min, and subsequently, Au NPs were added to the reaction mixtures. Spectra were recorded after allowing the aggregation for a fixed time interval of 10 min. Inset: resulting calibration curve. Error bars derived from a set of four experiments.

efficiency comparable to the aggregation of the NPs in the presence of cysteine/I^- with no co-added components (Figure S8, Supporting Information). The inhibited aggregation of the Au NPs was observed in the presence of acetylcholine, AChE, and ChOx. Evidently, the enzyme cascade is only activated in the presence of the two enzymes and the substrate acetylcholine. This indicates that in the presence of acetylcholine, the AChE/ChOx biocatalytically generated H_2O_2, and the subsequent oxidation of cysteine, leads to the inhibited aggregation of the NPs in the presence of the cysteine/I^-/Au NP reporter system.

From a practical point of view, it is, however, important to follow the inhibition of the activity of AChE. Toward this goal, we have examined the inhibition of AChE by 1,5-bis(4-allyldimethylammonium phenyl)-pentane-3-one dibromide (**6**), a common AChE inhibitor that mimics the functions of nerve gases.[56,57] In the presence of the inhibited AChE/ChOx bienzyme cascade system, the formation of H_2O_2 is blocked, thus leading to the effective aggregation of the NPs by the cysteine/I^-/Au NP reporter system. Accordingly, the AChE/ChOx cascaded biotransformation system was subjected to variable concentrations of the AChE inhibitor (**6**) at a fixed time interval of 120 min, and the content of the H_2O_2 generated by the different systems was probed by the aggregation of Au NPs by the cysteine/I^-/Au NP reporter system. Figure 6A–C depicts the time-dependent Au NP aggregation spectra upon the activation of the AChE/ChOx cascade in the presence of different concentrations of the AChE inhibitor (**6**). In these experiments, the AChE/ChOx cascade is activated in the presence of different concentrations of **6** for different reaction times. The resulting mixtures were then treated with the cysteine/I^- system for 20 min to allow the oxidation of cysteine to cystine, and subsequently, the Au NPs were introduced into the different systems to stimulate the aggregation of the Au NPs for a fixed time interval of 10 min. Figure 6A–C represents the recorded spectra after this time interval of aggregation. Figure 6D summarizes the time-dependent absorption changes of the Au NP aggregates formed by the AChE/ChOx cascade in the presence of different concentrations of **6**. Figure S9 (Supporting Information) depicts the effect of different concentrations of AChE inhibitor **6** on the AChE-stimulated aggregation of the Au NPs. In these experiments, the AChE/ChOx cascade, in the presence of variable concentrations of **6**, is activated in the presence of the cysteine/I^- system for a fixed time interval of 120 min. The resulting reaction mixtures were subjected to the cysteine/I^- reporter system for 20 min, and subsequently, Au NPs were added to the reaction mixtures and their degree of aggregation was followed spectroscopically after a fixed time interval of 10 min. Evidently, as the concentration of the inhibitor increases, the aggregation process is inhibited, consistent with the lower yield of H_2O_2 that leads to the inefficient oxidation of cysteine to cystine.

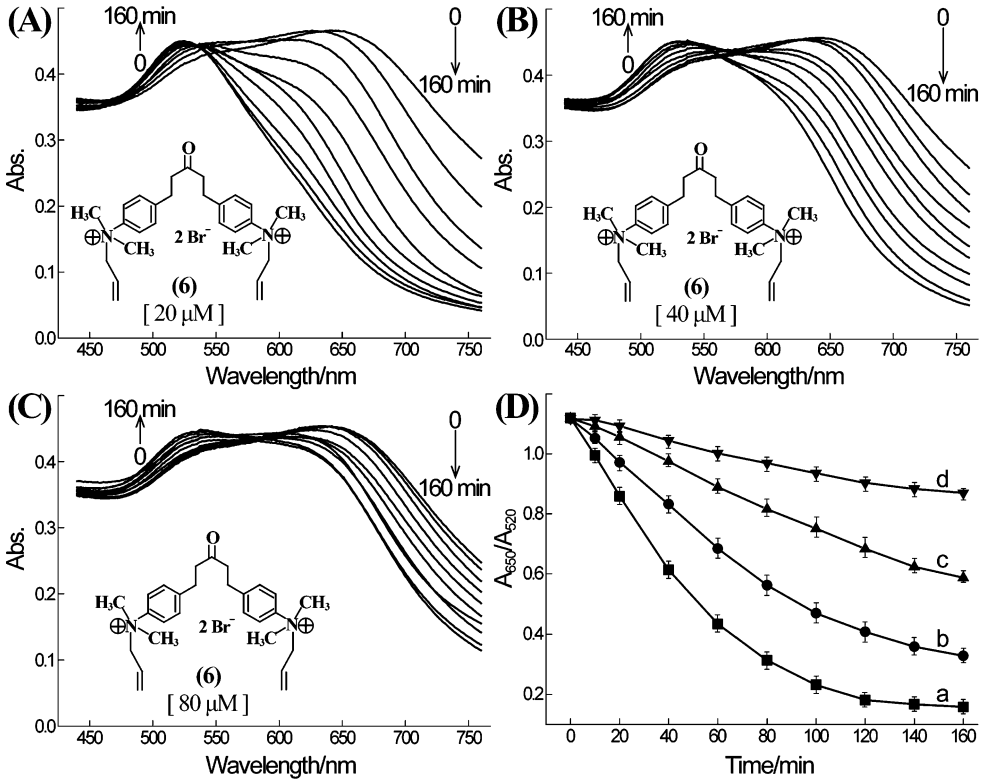

Figure 6. Aggregation spectra of the Au NPs that probe the inhibition of the AChE/ChOx cascade by different concentrations of the inhibitor 6. In these experiments, the AChE/ChOx cascade is activated in the presence of acetylcholine, 400 μM, and different concentrations of the inhibitor 6: (A) 20, (B) 40, and (C) 80 μM for variable time intervals. The different samples were then subjected to the cysteine/I^- reporter system for a time interval of 20 min, and subsequently, the Au NPs were injected into the respective sample and allowed to aggregate for a time interval of 10 min. (D) Time-dependent spectral changes of the aggregated Au NP systems formed in the presence of different concentrations of 6: (a) 0, (b) 20, (c) 40, and (d) 80 μM, following the procedure outlined in (A–C). Error bars derived from a set of four experiments.

CONCLUSIONS

In conclusion, the present study has developed a sensitive method for the detection of H_2O_2 through the aggregation of Au NPs by the cysteine/I^-/Au NP reporter system. This H_2O_2 detection platform was then implemented to detect glucose (through the GOx-catalyzed oxidation of glucose that generates H_2O_2) and to analyze an inhibitor of AChE (by following the H_2O_2 generated by the AChE/ChOx cascade). The significance of the results rests on the high sensitivity for the detection of H_2O_2. This allows the detection of low concentrations of H_2O_2 present or generated by low concentrations of substrates in biological fluids. For example, the noninvasive detection of glucose in saliva is an interesting challenge for diabetes management (concentrations of glucose in saliva are *ca.* 1% of the concentrations of glucose in blood and are in the range of 8 to 200 μM). We find that the cysteine-mediated aggregation of the Au NPs by the GOx/glucose system is adequate for monitoring glucose levels in saliva, Figure S10, Supporting Information, thus suggesting the possible noninvasive detection of glucose in biological fluids.

EXPERIMENTAL SECTION

Materials and Reagents. 4-(2-Hydroxyethyl)piperazine-1-ethanesulfonic acid sodium salt (HEPES), chloroauric acid ($HAuCl_4 \cdot 3H_2O$), trisodium citrate, cysteine, glucose, hydrogen peroxide, glucose oxidase (GOx), acetylcholine, sodium iodide, 1,5-bis-(4-allyldimethylammonium phenyl)pentane-3-one dibromide, choline oxidase (ChOx), and acetylcholine esterase (AChE) were purchased from Sigma-Aldrich. Ultrapure water from a NANOpure Diamond (Barnstead Int., Dubuque, IA) source was used throughout the experiments.

Synthesis of Au NPs. The Au NPs with an average diameter of 13 nm were prepared using the citrate reduction method.[58] Briefly, a solution of sodium citrate (10 mL; 38 mM) was added to a rapidly stirred boiling aqueous solution of $HAuCl_4$ (100 mL; 1 mM). After 30 min of boiling, the red mixture was allowed to cool to room temperature, and the Au NPs were collected by filtering through a 0.45 μm membrane to remove the precipitate. Finally, 50 mL of Au NPs was mixed with 2 mL of 1% surfactant Tween-20 to yield well-dispersed Au NPs and was stored in a refrigerator at 4 °C. The concentration of the prepared Au NP dispersion was determined with UV–vis spectrometry reported previously and found to be 12 nM. It should be noted that the Tween-20 additive stabilizes the individual as well as the aggregated Au NPs.

Optical Colorimetric Detection Platform Based on Au NPs. Absorbance measurements of Au NPs were performed using a

Shimadzu UV-2401PC UV−vis spectrophotometer. A 200 μL measurement cell was used for all the experiments.

For colorimetric assay of H_2O_2, cysteine (20 μM) was incubated with sodium iodide (0.2 μM) and different concentrations of H_2O_2 for 20 min in HEPES buffer solution (100 mM, pH 7.0). Then 100 μL of the resulting mixture was added to 100 μL of the Au NP solution (12 nM), and the system was allowed to react for 10 min to induce aggregation.

For colorimetric assay of glucose, GOx (0.2 μM) was incubated with different concentrations of glucose in 96 μL HEPES buffer solution (100 mM, pH 7.0) for 60 min. Then cysteine (2 μL, 1 mM) and sodium iodide (2 μL, 10 μM) were added to the GOx/glucose mixture, and this system was allowed to react for 20 min. Finally, 100 μL of the resulting mixture was added to 100 μL of the prepared Au NP solution (12 nM) for 10 min.

For probing the biocatalytic process of the AChE/ChOx bienzyme cascade, different concentrations of acetylcholine were incubated with AChE (0.5 μM) and ChOx (1.0 μM) for 120 min in 96 μL HEPES buffer solution (100 mM, pH 7.4, including 20 mM $MgCl_2$). Then cysteine (2 μL, 1 mM) and sodium iodide (2 μL, 10 μM) were added to the AChE/ChOx/acetylcholine reaction mixture, and this system was allowed to react for 20 min. Finally, 100 μL of the resulting mixture was added to 100 μL of the prepared Au NP solution (12 nM), and the NPs were allowed to aggregate for 10 min.

Conflict of Interest: The authors declare no competing financial interest.

Acknowledgment. This research was supported by the Office of Naval Research (ONR), USA.

Supporting Information Available: The possible mechanism and the optimization of the I^--catalyzed oxidization of cysteine to cystine by H_2O_2, time-dependent H_2O_2-generating biocatalytic reactions through the aggregation of the Au NPs, all the control experiments, and analysis of glucose in artificial saliva samples. This material is available free of charge *via* the Internet at http://pubs.acs.org.

REFERENCES AND NOTES

1. Sperling, R. A.; Gil, P. R.; Zhang, F.; Zanella, M.; Parak, W. J. Biological Applications of Gold Nanoparticles. *Chem. Soc. Rev.* **2008**, *37*, 1896–1908.
2. Saha, K.; Agasti, S. S.; Kim, C.; Li, X.; Rotello, V. M. Gold Nanoparticles in Chemical and Biological Sensing. *Chem. Rev.* **2012**, *112*, 2739–2779.
3. Jans, H.; Huo, Q. Gold Nanoparticle-Enabled Biological and Chemical Detection and Analysis. *Chem. Soc. Rev.* **2012**, *41*, 2849–2866.
4. Su, K. H.; Wei, Q. H.; Zhang, X.; Mock, J. J.; Smith, D. R.; Schultz, S. Interparticle Coupling Effects on Plasmon Resonances of Nanogold Particles. *Nano Lett.* **2003**, *3*, 1087–1090.
5. Ghosh, S. K.; Pal, T. Interparticle Coupling Effect on the Surface Plasmon Resonance of Gold Nanoparticles: From Theory to Applications. *Chem. Rev.* **2007**, *107*, 4797–4862.
6. Liu, J.; Lu, Y. Fast Colorimetric Sensing of Adenosine and Cocaine Based on a General Sensor Design Involving Aptamers and Nanoparticles. *Angew. Chem., Int. Ed.* **2005**, *45*, 90–94.
7. Shenton, W.; Davis, S. A.; Mann, S. Directed Self-Assembly of Nanoparticles into Macroscopic Materials Using Antibody–Antigen Recognition. *Adv. Mater.* **1999**, *11*, 449–452.
8. Otsuka, H.; Akiyama, Y.; Nagasaki, Y.; Kataoka, K. Quantitative and Reversible Lectin-Induced Association of Gold Nanoparticles Modified with α-Lactosyl-ω-Mercapto-Poly(ethylene glycol). *J. Am. Chem. Soc.* **2001**, *123*, 8226–8230.
9. Liu, J.; Mendoza, S.; Román, E.; Lynn, M. J.; Xu, R.; Kaifer, A. E. Cyclodextrin-Modified Gold Nanospheres. Host–Guest Interactions at Work to Control Colloidal Properties. *J. Am. Chem. Soc.* **1999**, *121*, 4304–4305.
10. Lin, S. Y.; Liu, S. W.; Lin, C. M.; Chen, C. H. Recognition of Potassium Ion in Water by 15-Crown-5 Functionalized Gold Nanoparticles. *Anal. Chem.* **2002**, *74*, 330–335.
11. Boal, A. K.; Ilhan, F.; DeRouchey, J. E.; Thurn-Albrecht, T.; Russell, T. P.; Rotello, V. M. Self-Assembly of Nanoparticles into Structured Spherical and Network Aggregates. *Nature* **2000**, *404*, 746–748.
12. Balogh, D.; Zhang, Z.; Cecconello, A.; Vavra, J.; Severa, L.; Teply, F.; Willner, I. Helquat-Induced Chiroselective Aggregation of Au NPs. *Nano Lett.* **2012**, *12*, 5835–5839.
13. Jiang, Y.; Zhao, H.; Zhu, N.; Lin, Y.; Yu, P.; Mao, L. A Simple Assay for Direct Colorimetric Visualization of Trinitrotoluene at Picomolar Levels Using Gold Nanoparticles. *Angew. Chem., Int. Ed.* **2008**, *47*, 8601–8604.
14. Li, H.; Rothberg, L. Colorimetric Detection of DNA Sequences Based on Electrostatic Interactions with Unmodified Gold Nanoparticles. *Proc. Natl. Acad. Sci. U.S.A.* **2004**, *101*, 14036–14039.
15. Rosi, N. L.; Mirkin, C. A. Nanostructures in Biodiagnostics. *Chem. Rev.* **2005**, *105*, 1547–1562.
16. Zhao, W.; Chiuman, W.; Brook, M. A.; Li, Y. Simple and Rapid Colorimetric Biosensors Based on DNA Aptamer and Noncrosslinking Gold Nanoparticle Aggregation. *ChemBioChem* **2007**, *8*, 727–731.
17. Wang, J.; Wang, L.; Liu, X.; Liang, Z.; Song, S.; Li, W.; Li, G.; Fan, C. A Gold Nanoparticle-Based Aptamer Target Binding Readout for ATP Assay. *Adv. Mater.* **2007**, *19*, 3943–3946.
18. Lee, J. S.; Han, M. S.; Mirkin, C. A. Colorimetric Detection of Mercuric Ion (Hg^{2+}) in Aqueous Media Using DNA-Functionalized Gold Nanoparticles. *Angew. Chem., Int. Ed.* **2007**, *46*, 4093–4106.
19. Li, D.; Wieckowska, A.; Willner, I. Optical Analysis of Hg^{2+} Ions by Oligonucleotide–Gold-Nanoparticle Hybrids and DNA-Based Machines. *Angew. Chem., Int. Ed.* **2008**, *47*, 3927–3931.
20. Liu, J.; Lu, Y. A Colorimetric Lead Biosensor Using DNAzyme-Directed Assembly of Gold Nanoparticles. *J. Am. Chem. Soc.* **2003**, *125*, 6642–6643.
21. Hazarika, P.; Ceyhan, B.; Niemeyer, C. M. Reversible Switching of DNA–Gold Nanoparticle Aggregation. *Angew. Chem., Int. Ed.* **2004**, *43*, 6469–6471.
22. Kim, Y.; Johnson, R. C.; Hupp, J. T. Gold Nanoparticle-Based Sensing of "Spectroscopically Silent" Heavy Metal Ions. *Nano Lett.* **2001**, *1*, 165–167.
23. He, L.; Musick, M. D.; Nicewarner, S. R.; Salinas, F. G.; Benkovie, S. J.; Natan, M. J.; Keating, C. D. Colloidal Au-Enhanced Surface Plasmon Resonance for Ultrasensitive Detection of DNA Hybridization. *J. Am. Chem. Soc.* **2000**, *122*, 9071–9077.
24. Medintz, I. L.; Uyeda, H. T.; Goldman, E. R.; Mattoussi, H. Quantum Dot Bioconjugates for Imaging, Labelling and Sensing. *Nat. Mater.* **2005**, *4*, 435–446.
25. Wang, F.; Liu, X.; Willner, I. Integration of Photoswitchable Proteins, Photosynthetic Reaction Centers and Semiconductor/Biomolecule Hybrids with Electrode Supports for Optobioelectronic Applications. *Adv. Mater.* **2013**, *25*, 349–377.
26. Riskin, M.; Tel-Vered, R.; Bourenko, T.; Granot, E.; Willner, I. Imprinting of Molecular Recognition Sites through Electropolymerization of Functionalized Au Nanoparticles: Development of an Electrochemical TNT Sensor Based on π-Donor–Acceptor Interactions. *J. Am. Chem. Soc.* **2008**, *130*, 9726–9733.
27. Riskin, M.; Tel-Vered, R.; Lioubashevski, O.; Willner, I. Ultrasensitive Surface Plasmon Resonance Detection of Trinitrotoluene by a Bis-aniline-Cross-Linked Au Nanoparticles Composite. *J. Am. Chem. Soc.* **2009**, *131*, 7368–7378.
28. Matsui, J.; Akamatsu, K.; Hara, N.; Miyoshi, D.; Nawafune, H.; Tamaki, K.; Sugimoto, N. SPR Sensor Chip for Detection of Small Molecules Using Molecularly Imprinted Polymer with Embedded Gold Nanoparticles. *Anal. Chem.* **2005**, *77*, 4282–4285.
29. Golub, E.; Pelossof, G.; Freeman, R.; Zhang, H.; Willner, I. Electrochemical, Photoelectrochemical, and Surface Plasmon Resonance Detection of Cocaine Using Supramolecular Aptamer Complexes and Metallic or Semiconductor Nanoparticles. *Anal. Chem.* **2009**, *81*, 9291–9298.

30. Shipway, A. N.; Lahav, M.; Blonder, R.; Willner, I. Bis-bipyridinium Cyclophane Receptor−Au Nanoparticle Superstructures for Electrochemical Sensing Applications. *Chem. Mater.* **1999**, *11*, 13–15.
31. Freeman, R.; Finder, T.; Bahshi, L.; Willner, I. β-Cyclodextrin-Modified CdSe/ZnS Quantum Dots for Sensing and Chiroselective Analysis. *Nano Lett.* **2009**, *9*, 2073–2076.
32. Jin, W. J.; Fernandez-Arguelles, M. T.; Costa-Fernandez, J. M.; Pereiro, R.; Sanz-Medel, A. Photoactivated Luminescent CdSe Quantum Dots as Sensitive Cyanide Probes in Aqueous Solutions. *Chem. Commun.* **2005**, 883–885.
33. Cordes, D. B.; Gamsey, S.; Singaram, B. Fluorescent Quantum Dots with Boronic Acid Substituted Viologens To Sense Glucose in Aqueous Solution. *Angew. Chem., Int. Ed.* **2006**, *45*, 3829–3832.
34. Freeman, R.; Finder, T.; Bahshi, L.; Gill, R.; Willner, I. Functionalized CdSe/ZnS QDs for the Detection of Nitroaromatic or RDX Explosives. *Adv. Mater.* **2012**, *24*, 6416–6421.
35. Zayats, M.; Baron, R.; Popov, I.; Willner, I. Biocatalytic Growth of Au Nanoparticles: From Mechanistic Aspects to Biosensors Design. *Nano Lett.* **2005**, *5*, 21–25.
36. Luo, W.; Zhu, C.; Su, S.; Li, D.; He, Y.; Huang, Q.; Fan, C. Self-Catalyzed, Self-Limiting Growth of Glucose Oxidase-Mimicking Gold Nanoparticles. *ACS Nano* **2010**, *4*, 7451–7458.
37. Willner, I.; Baron, R.; Willner, B. Growing Metal Nanoparticles by Enzymes. *Adv. Mater.* **2006**, *18*, 1109–1120.
38. Bahshi, L.; Freeman, R.; Gill, R.; Willner, I. Optical Detection of Glucose by Means of Metal Nanoparticles or Semiconductor Quantum Dots. *Small* **2009**, *5*, 676–680.
39. Jin, L.; Shang, L.; Guo, S.; Fang, Y.; Wen, D.; Wang, L.; Yin, J.; Dong, S. Biomolecule-Stabilized Au Nanoclusters as a Fluorescence Probe for Sensitive Detection of Glucose. *Biosens. Bioelectron.* **2011**, *26*, 1965–1969.
40. Liu, X.; Wang, F.; Niazov-Elkan, A.; Guo, W.; Willner, I. Probing Biocatalytic Transformations with Luminescent DNA/Silver Nanoclusters. *Nano Lett.* **2013**, *13*, 309–314.
41. Ben-Amram, Y.; Riskin, M.; Willner, I. Selective and Enantioselective Analysis of Mono- and Disaccharides Using Surface Plasmon Resonance Spectroscopy and Imprinted Boronic Acid-Functionalized Au Nanoparticle Composites. *Analyst* **2010**, *135*, 2952–2959.
42. Xiao, Q.; Shang, F.; Xu, X.; Li, Q.; Lu, C.; Lin, J. M. Specific Detection of Cysteine and Homocysteine in Biological Fluids by Tuning the pH Values of Fluorosurfactant-Stabilized Gold Colloidal Solution. *Biosens. Bioelectron.* **2011**, *30*, 211–215.
43. Lu, C.-H.; Wang, Y.-W.; Ye, S.-L.; Chen, G.-N.; Yang, H.-H. Ultrasensitive Detection of Cu^{2+} with the Naked Eye and Application in Immunoassays. *NPG Asia Mater.* **2012**, *4*, e10.
44. Kirihara, M.; Asai, Y.; Ogawa, S.; Noguchi, T.; Hatano, A.; Hirai, Y. A Mild and Environmentally Benign Oxidation of Thiols to Disulfides. *Synthesis* **2007**, *21*, 3286–3289.
45. Miao, Y.; He, N.; Zhu, J.-J. History and New Developments of Assays for Cholinesterase Activity and Inhibition. *Chem. Rev.* **2010**, *110*, 5216–5234.
46. Perry, E.; Walker, M.; Grace, J.; Perry, R. Acetylcholine in Mind: A Neurotransmitter Correlate of Consciousness? *Trends Neurosci.* **1999**, *22*, 273–280.
47. Pauluhn, J.; Machemer, L.; Kimmerle, G. Effects of Inhaled Cholinesterase Inhibitors on Bronchial Tonus and on Plasma and Erythrocyte Acetylcholine Esterase Activity in Rats. *Toxicology* **1987**, *46*, 177–190.
48. Virel, A.; Saa, L.; Pavlov, V. Modulated Growth of Nanoparticles. Application for Sensing Nerve Gases. *Anal. Chem.* **2009**, *81*, 268–272.
49. Pavlov, V.; Xiao, Y.; Willner, I. Inhibition of the Acetycholine Esterase-Stimulated Growth of Au Nanoparticles: Nanotechnology-Based Sensing of Nerve Gases. *Nano Lett.* **2005**, *5*, 649–653.
50. Riklin, A.; Willner, I. Glucose and Acetylcholine Sensing Multilayer Enzyme Electrodes of Controlled Enzyme Layer Thickness. *Anal. Chem.* **1995**, *67*, 4118–4126.
51. Pardo-Yissar, V.; Katz, E.; Wasserman, J.; Willner, I. Acetylcholine Esterase-Labeled CdS Nanoparticles on Electrodes: Photoelectrochemical Sensing of the Enzyme Inhibitors. *J. Am. Chem. Soc.* **2003**, *125*, 622–623.
52. Wang, M.; Gu, X.; Zhang, G.; Zhang, D.; Zhu, D. Continuous Colorimetric Assay for Acetylcholinesterase and Inhibitor Screening with Gold Nanoparticles. *Langmuir* **2009**, *25*, 2504–2507.
53. Sun, J.; Guo, L.; Bao, Y.; Xie, J. A Simple, Label-Free AuNPs-Based Colorimetric Ultrasensitive Detection of Nerve Agents and Highly Toxic Organophosphate Pesticide. *Biosens. Bioelectron.* **2011**, *28*, 152–157.
54. Gill, R.; Bahshi, L.; Freeman, R.; Willner, I. Optical Detection of Glucose and Acetylcholine Esterase Inhibitors by H_2O_2-Sensitive CdSe/ZnS Quantum Dots. *Angew. Chem., Int. Ed.* **2008**, *47*, 1676–1679.
55. Meng, X.; Wei, J.; Ren, X.; Ren, J.; Tang, F. A Simple and Sensitive Fluorescence Biosensor for Detection of Organophosphorus Pesticides Using H_2O_2-Sensitive Quantum Dots/Bi-enzyme. *Biosens. Bioelectron.* **2013**, *47*, 402–407.
56. Dipatre, P. L.; Mathes, C. W.; Butcher, L. L. Differential Visualization of Cholinesterasic Neuronal Somata and Fibers by Use of Modifications of Acetylcholinesterase Pharmacohistochemistry. *J. Histochem. Cytochem.* **1993**, *41*, 129–135.
57. Dupree, J. L.; Bigbee, J. W. Retardation of Neuritic Outgrowth and Cytoskeletal Changes Accompany Acetylcholinesterase Inhibitor Treatment in Cultured Rat Dorsal Root Ganglion Neurons. *J. Neurosci. Res.* **1994**, *39*, 567–575.
58. Grabar, K. C.; Freeman, R. G.; Hommer, M. B.; Natan, M. J. Preparation and Characterization of Au Colloid Monolayers. *Anal. Chem.* **1995**, *67*, 735–743.